ACS NANO

www.acsnano.org

ARTICLE

Spin Coating Promotes the Epitaxial Growth of AgCN Microwires on 2D Materials

Jimin Ham, Jaemook Lim, Sukjoon Hong, and Won Chul Lee*

Cite This: *ACS Nano* 2022, 16, 20521−20532

Read Online

ACCESS | Metrics & More | Article Recommendations | Supporting Information

ABSTRACT: Epitaxial growth of inorganic crystals on 2D materials is expected to greatly advance nanodevices and nanocomposites. However, because pristine surfaces of 2D materials are chemically inert, it is difficult to grow inorganic crystals epitaxially on 2D materials. Previously, successful results were achieved only by vapor-phase deposition at high temperature, and solution-based deposition including spin coating made the epitaxial growth unaligned, sparse, or nonuniform on 2D materials. Here, we show that solvent-controlled spin coating can uniformly deposit a dense layer of epitaxial AgCN microwires onto various 2D materials. Adding ethanol to an aqueous AgCN solution facilitates uniform formation of the thin supersaturated solution layer during spin coating, which promotes heterogeneous crystal nucleation on 2D material surfaces over homogeneous nucleation in the bulk solution. Microscopic analysis confirms highly aligned, uniform, and dense growth of epitaxial AgCN microwires on graphene, MoS_2, hBN, WS_2, and WSe_2. The epitaxial microwires, which are optically observable and chemically removable, enable crystallographic mapping of grains in millimeter-sized polycrystalline graphene as well as precise control of twist angles (<~1°) in van der Waals heterostructures. In addition to these practical applications, our study demonstrates the potential of 2D materials as epitaxial templates even in spin coating of inorganic crystals.

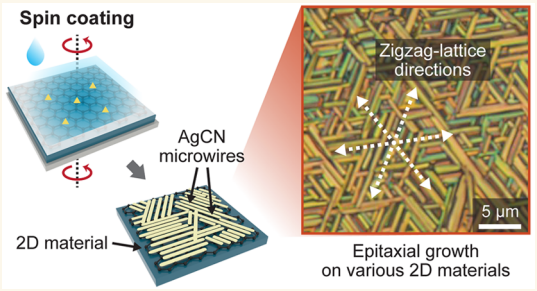

KEYWORDS: *spin coating, epitaxial growth, van der Waals epitaxy, silver cyanide, 2D materials, van der Waals heterostructures*

Heteroepitaxial growth on 2D materials is a promising approach for producing nanoelectronic devices and nanocomposite materials such as 2D/2D or 2D/3D heterostructures.[1−3] The atomic alignment between an epitaxial crystal and the underlying 2D material often leads to an advanced class of functionalities, as has previously been demonstrated with organic molecules epitaxially aligned on 2D materials.[3,4] However, because pristine 2D materials have chemically inert surfaces without any dangling bond, it is difficult to grow inorganic crystals epitaxially on 2D materials. In the traditional heteroepitaxy (such as silicon or III−V compound epitaxy on sapphire), bulk material surfaces periodically exposing dangling bonds provide a large free-energy difference for spontaneously driving the epitaxial growth,[5−7] but heteroepitaxy on 2D materials requires a relatively high energy supplied into the epitaxial growth reaction. As a result, successful cases of heteroepitaxy on 2D materials, so-called van der Waals epitaxy,[8] have been mostly achieved by vapor-phase deposition at high temperature.[9−16] Solution-phase synthesis, incubating 2D materials immersed in or floated on precursor solutions, shows only a few examples of the epitaxial growth,[17−22] and moreover, the synthesized crystals are either poorly aligned or sparsely distributed on 2D materials. A general consensus is that solution-phase incubation is suitable for the nanoparticle growth nucleated at defects of 2D materials,[23] while is unsuitable for the epitaxial growth on pristine surfaces of 2D materials.

Spin coating and drop casting are efficient alternatives for depositing solid materials from solution-phase precursors,[7,24−26] but these two methods, in which solvent evaporation drives the process rather kinetically than thermodynamically, are also considered unsuitable for the epitaxial growth on 2D materials. A few previous reports have presented that spin coating and thermal incubation of perovskites on 2D materials form epitaxial films,[27−30] whose alignments are clearly poorer than those of perovskite films spin-coated on bulk material surfaces (metal or strontium titanate substrates).[7] Drop casting of epitaxial inorganic crystals on 2D materials has been achieved in only two types of previous studies. The first one is gold nanowire epitaxy on MoS_2,[31] in which large deviations of crystallographic

Received: July 14, 2022
Accepted: December 2, 2022
Published: December 7, 2022

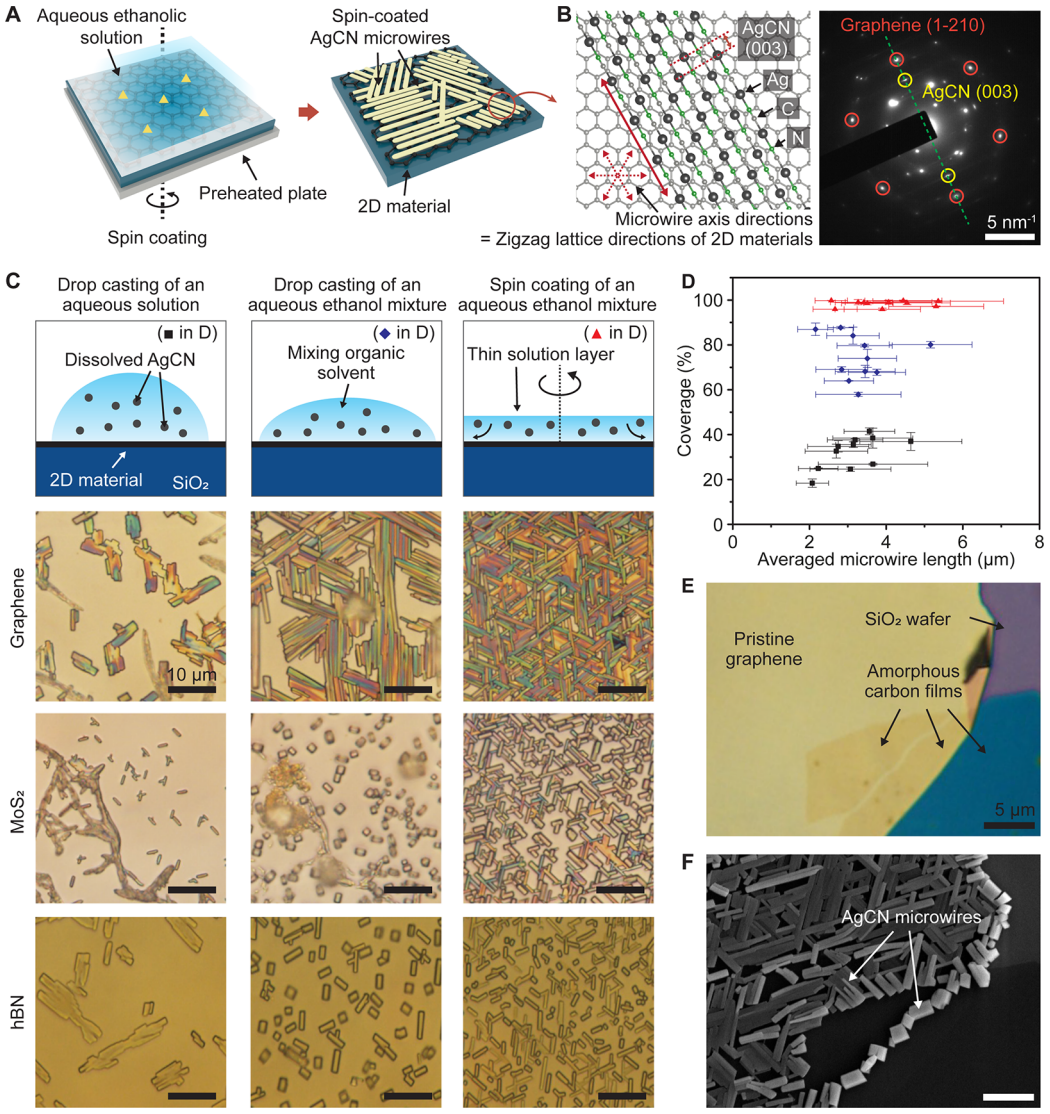

Figure 1. Epitaxial growth of AgCN microwires on various 2D materials. (A) Schematic of the spin-coating process using a AgCN solution dissolved in an aqueous ethanol mixture. (B) Atomic configuration (left) and SAED pattern (right) of AgCN epitaxially aligned on graphene. (C) Growth methods and optical images of AgCN microwires grown on graphene (top), MoS_2 (middle), and hBN (bottom) by three synthesis methods: drop casting of an aqueous solution (left), drop casting of an aqueous ethanol mixture (middle), and spin coating of an aqueous ethanol mixture (right). Microwires grown on WS_2 and WSe_2 are shown in Figure S2. (D) Areal coverages versus averaged lengths of AgCN microwires grown on graphene by the three synthesis methods. (E and F) Optical and SEM images of a graphene sample before (E) and after (F) microwire growth on four different surfaces (pristine graphene, graphene edges, amorphous carbon, and silicon oxide).

orientations are observed. The other type is the epitaxial growth of metal cyanide complexes on 2D materials.[32−38] After the discovery of solution-phase epitaxy of gold(I) cyanide (AuCN) on graphene,[19] five kinds of metal cyanides (AuCN,[32−34] AgCN,[35−37] CuCN,[37] $Cu_{0.5}Au_{0.5}CN$,[36] and $Au_{1/2}Ag_{1/2}CN$)[38] have been confirmed to grow epitaxially on various 2D materials (graphene, MoS_2, hBN, and so on) using drop casting of aqueous solutions. However, all the growth results of this metal cyanide epitaxy are highly unstable and nonuniform due to intrinsic limitations of drop casting: Most of the substrate areas either contain a few epitaxial crystals with extremely low areal densities or are covered by highly concentrated aggregates of nonepitaxial crystals formed from the bulk solution. Therefore, it is fair to say that spin coating and drop casting show poor alignments, low areal densities, or nonuniform deposition in the epitaxial growth on 2D materials.

Here, we demonstrate that a dense layer of epitaxial AgCN microwires can be deposited uniformly onto various 2D materials by spin coating of a water−ethanol mixed solution. Both controlling solvent properties with the ethanol addition and applying the spin-coating method facilitate uniform and conformal formation of the thin supersaturated solution layer, promoting heterogeneous crystal nucleation on 2D material surfaces over homogeneous nucleation in the bulk solution. We compare the present method to drop casting of aqueous or water−ethanol mixed solutions and thus confirm that our method offers highly aligned, uniform, and dense growth of epitaxial AgCN microwires on various 2D materials (graphene, MoS_2, hBN, WS_2, and WSe_2). Because the spin-coated microwires are observable with conventional optical microscopy and removable with simple wet chemistry, we can apply our method to large-area crystallographic mapping of grains in millimeter-sized polycrystalline graphene as well as precise

https://doi.org/10.1021/acsnano.2c06963
ACS Nano 2022, 16, 20521−20532

control of twist angles (<~1°) in the fabrication of van der Waals heterostructures. In addition to these two practical applications, our study demonstrates the possibility of using 2D materials as templates for the epitaxial growth, even with spin coating of inorganic crystals.

RESULTS AND DISCUSSION

Spin Coating of Epitaxial AgCN Microwires on 2D Materials. The main claim of this study is that spin coating of AgCN dissolved in an aqueous ethanol mixture (Figure 1A) can form a dense layer of epitaxially grown microwires on various 2D materials, which is clearly verified from microscopic images of typical samples (Figure 1C; Figures S1 and S2). Figure 1C and Figure S2 show AgCN microwires synthesized on five types of 2D materials (graphene, MoS_2, hBN, WS_2, and WSe_2) using three different methods (drop casting of an aqueous solution, drop casting of an aqueous ethanol mixture, and spin coating of an aqueous ethanol mixture). Although all three methods applied onto the five 2D materials can form AgCN microwires preferentially oriented with 3-fold rotational symmetry (Figure 1B and Figure S3 describe the epitaxial relationship), their uniformities and areal densities are largely different. Drop casting of an aqueous AgCN solution, the conventional method,[35−37] leads to sparse and nonuniform growth of microwires on all five 2D materials (left images in Figure 1C; Figures S1A and S2A). In addition, there exist defocused or irregularly shaped particles on the 2D materials, and these particles are nonepitaxial crystals formed by homogeneous nucleation in the bulk solution. The above limitations come from water being a poor solvent for drop casting due to its low vapor pressure, inconsistent surface affinity, and large surface tension.[39] Mixing organic solvents into an aqueous solution can control these solvent properties suitable for the evaporation-driven deposition process.[24,25] Therefore, we change the solvent to an aqueous ethanol mixture, and then the drop-casting results show improved uniformities and areal densities (centered images in Figure 1C; Figures S1B and S2B). However, these samples still have empty areas on 2D materials and nonepitaxial crystals formed by homogeneous nucleation (defocused particles in the images). Spin coating of an aqueous ethanol mixture uniformly forms AgCN epitaxial microwires which cover almost entire areas of the underlying 2D materials (right images in Figure 1C; Figures S1C, S2C, and S4A). The quantitative comparison using 11 graphene samples in Figure 1D clearly shows this improvement, where coverage ratios (the ratios of microwire areas to entire graphene areas) are 35.1 ± 3.2%, 75.2 ± 3.3%, and 98.5 ± 3.9% for the three growth methods, respectively. We also investigate the present spin-coating method under various conditions such as the number of graphene layers, substrate types, rotational acceleration, and ethanol contents, which are described in the subsection "Effects of Microwire Growth Conditions". In particular, we note that spin coating of an aqueous AgCN solution synthesizes no microwire onto 2D materials (Figure S5). The combination of spin coating and an aqueous ethanolic solvent is a key part for the dense and uniform growth of epitaxial microwires on 2D materials.

Underlying Mechanisms of Spin Coating and Epitaxial Alignment. The mechanistic understanding of the spin-coating process enables us to explain underlying principles of dense and uniform growth of epitaxial AgCN microwires (Figure S6). In either drop casting or spin coating, heterogeneous crystal nucleation occurs first at the interface between a dropped solution and a 2D material surface, and then the crystalline nuclei on the surface continue to grow until the solvent completely evaporates. We experimentally evaluate the effects of these two steps of nucleation and growth by measuring areal densities of nucleation sites (Figures S7 and S8) and microwire sizes (Figure 1D). The areal density of nucleation sites is increased in the present spin-coating method (0.378 ± 0.050 ea/μm^2), compared to those in the two drop-casting methods (0.074 ± 0.020 ea/μm^2 and 0.179 ± 0.035 ea/μm^2). On the other hand, the microwire sizes, which are decided by the growth stage, present no noticeable difference among the three deposition methods, as shown in the lengths (3.2 ± 0.8 μm, 3.3 ± 0.7 μm, and 3.9 ± 0.9 μm, respectively) and the 2D-projected areas (2.5 ± 1.0 μm^2, 2.6 ± 0.9 μm^2, and 2.8 ± 0.9 μm^2, respectively). The above observations indicate that the improved density and uniformity in the present spin-coating method originate from the nucleation stage, not from the growth stage. This improved nucleation can be driven by the following two mechanisms, which were presented in the previous study[7] originally demonstrating spin-coated epitaxial films on bulk material substrates. First, the thin supersaturated solution layer formed during spin coating promotes heterogeneous crystal nucleation on 2D material surfaces over homogeneous nucleation in the bulk solution.[7] Compared to spin coating, drop-casting results (Figure S9) present many aggregates of irregularly shaped crystals from the bulk solution. Adding ethanol to the aqueous AgCN solution further facilitates uniform formation of the thin solution layer in the spin-coating process. The aqueous ethanolic mixture has a decreased kinematic viscosity, which reduces the solution thickness during spin coating. For example, kinematic viscosities of 0.01 $cm^2\ s^{-1}$ (water at 20 °C) and 0.03 $cm^2\ s^{-1}$ (4:6 aqueous ethanolic mixture at 20 °C) at a rotation rate of 3000 rpm generate hydrodynamic boundary layers of ~200 μm and ~120 μm, respectively. The aqueous ethanolic mixture also indicates improved affinities to both SiO_2 and graphene surfaces, as confirmed by contact angle measurements (water vs mixture = 65.3° vs 19.7° on SiO_2 and 73.2° vs 24.6° on graphene) in Figure S10. The low affinities of the aqueous solution would prevent spin coating from synthesizing microwires on the surfaces (Figure S5). Second, the other mechanism for promoting nucleation is that anion adsorption onto 2D material surfaces may lower the activation energy for heterogeneous nucleation.[7] In our reaction system, $Ag(CN)_2^-$ anions, which are dominant among silver cyanide species in the solution,[40] are expected to be preferentially adsorbed and then to grow to linear $Ag_n(CN)_{n+1}^-$ chains on pristine graphitic surfaces.[41,42] Specific adsorption of these anion families is likely to provide nucleation sites for heterogeneous crystallization, which is indirectly supported by the following control experiment (Figure 1E and F; Figure S11). We prepare a specimen providing four different types of surfaces for microwire growth (Figure 1E): pristine graphene in the middle of graphene flakes, graphene defects at the edge of the flakes, and two bulk materials presenting many dangling bonds (amorphous carbon and silicon oxide). After the spin coating, no microwire is formed on either amorphous carbon or silicon oxide surfaces, and the microwire density is uniform throughout the graphene domains and edges (Figure 1F). This result coincides well with the previous expectation that $Ag(CN)_2^-$ anions strongly interact with pristine graphitic surfaces. In addition, the result implies that the present spin-coating method can strengthen pre-existing affinity to promote

https://doi.org/10.1021/acsnano.2c06963
ACS Nano 2022, 16, 20521−20532

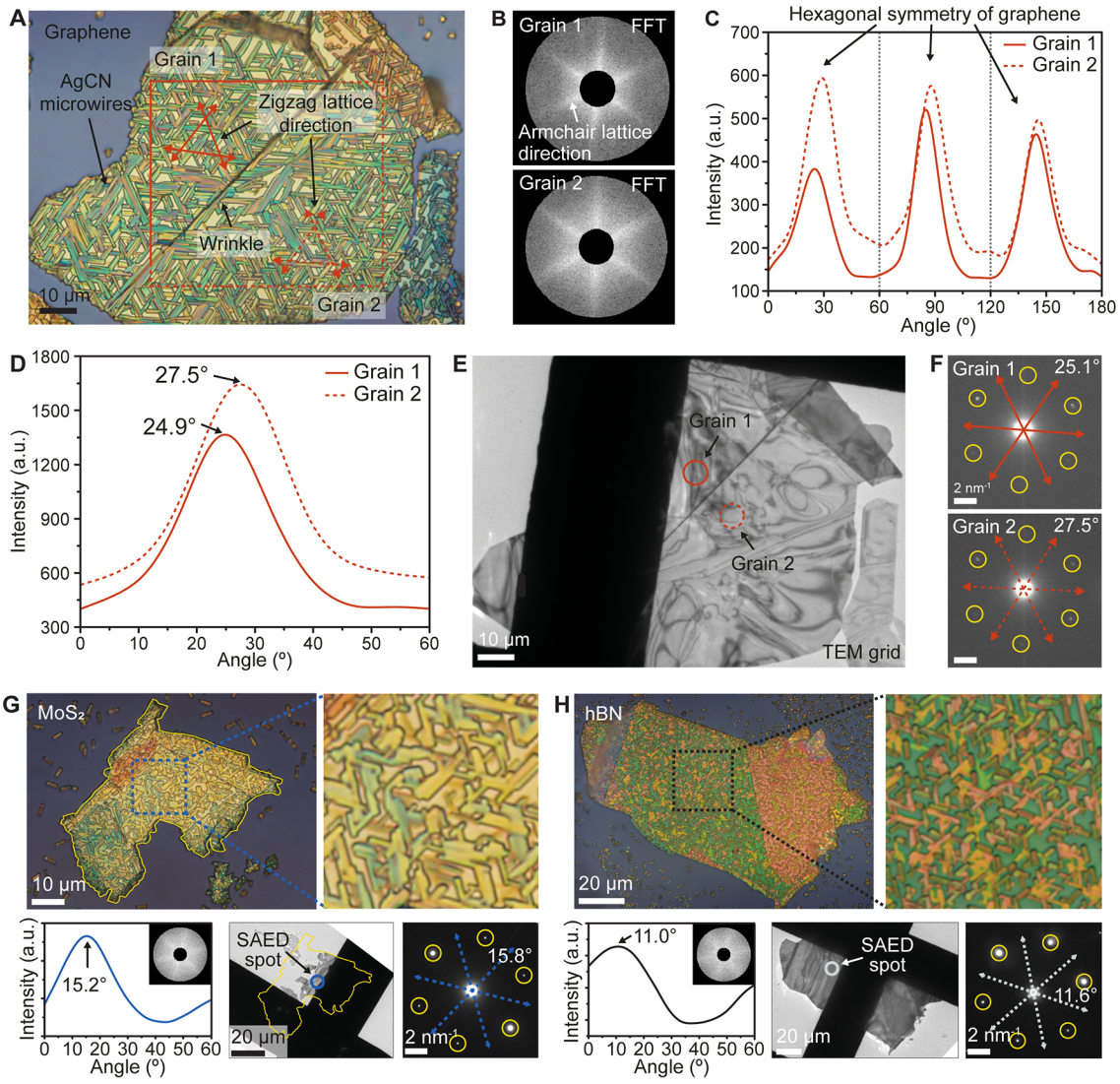

Figure 2. Optical observation of crystallographic orientations in three different 2D materials (graphene, MoS_2, and hBN) using spin-coated microwires. (A) Optical image of microwires grown on two grains of multilayered graphene separated by a wrinkle. (B) 2D fast Fourier transform (FFT) of microwire images on two grain areas in (A). Six-pointed asterisk (*) patterns indicate armchair lattice directions of the underlying graphene (orientations orthogonal to microwire axial directions). (C and D) Radial pixel intensities of (B), averaged along from the center at different angles. The angular directions are transformed from 0°−180° (C) to 0°−60° (D) based on the hexagonal symmetry. (E) TEM image of the graphene sample in (A) which is transferred onto a TEM grid after microwire removal. (F) SAED patterns from the two areas in (E). The yellow circles and the red arrows indicate armchair and zigzag lattice directions of graphene, respectively. (G and H) Identical experiments performed with MoS_2 (G) and hBN (H).

epitaxial growth but cannot generate epitaxial growth between two materials that have low affinity to each other. The expected mechanism of the present spin-coating process, discussed in this paragraph, is summarized in Figure S6.

Figure 1E and F also indicate that the AgCN microwires grow directly on chemically inert surfaces of pristine graphene, not on graphene defects, although most inorganic materials preferentially attach to dangling bonds such as 2D material edges and defects.[23] This uncommon characteristic can be explained with van der Waals epitaxy,[8] which is a heteroepitaxial relationship between two surfaces having no dangling bond. AgCN is named as a quasi-1D (quasi-one-dimensional) material: The atoms in a 1D chain of $[Ag-C\equiv N-]_n$ are bound to each other with strong covalent bonds, whereas the chains are held together via van der Waals forces to form a hexagonal crystal (Figure 1B; Figure S3).[43] Therefore, the AgCN surface along the 1D chains exposes no dangling bond, and this surface can generate van der Waals epitaxial interaction onto pristine surfaces of 2D materials. The observation of the 3-fold rotational symmetry in microwire orientations (Figure 1B, C, and F) clearly confirms the epitaxial alignment of AgCN onto lattice structures of pristine 2D material surfaces. The mechanism of this epitaxial alignment needs to be discussed further, because lattice matching, unlike conventional epitaxy, is generally not a main cause of van der Waals epitaxy.[8] Previous studies have shown that various metal cyanides including AuCN, AgCN, CuCN, $Cu_{0.5}Ag_{0.5}CN$, and $Au_{1/2}Ag_{1/2}CN$ present the alignment of 1D cyanide chains along the zigzag lattice directions of various 2D materials including graphene, hBN, MoS_2, WS_2, $MoTe_2$, and WTe_2.[19,32−38] The previous studies explained that the epitaxial alignment originates from orientation-dependent

https://doi.org/10.1021/acsnano.2c06963
ACS Nano 2022, 16, 20521−20532

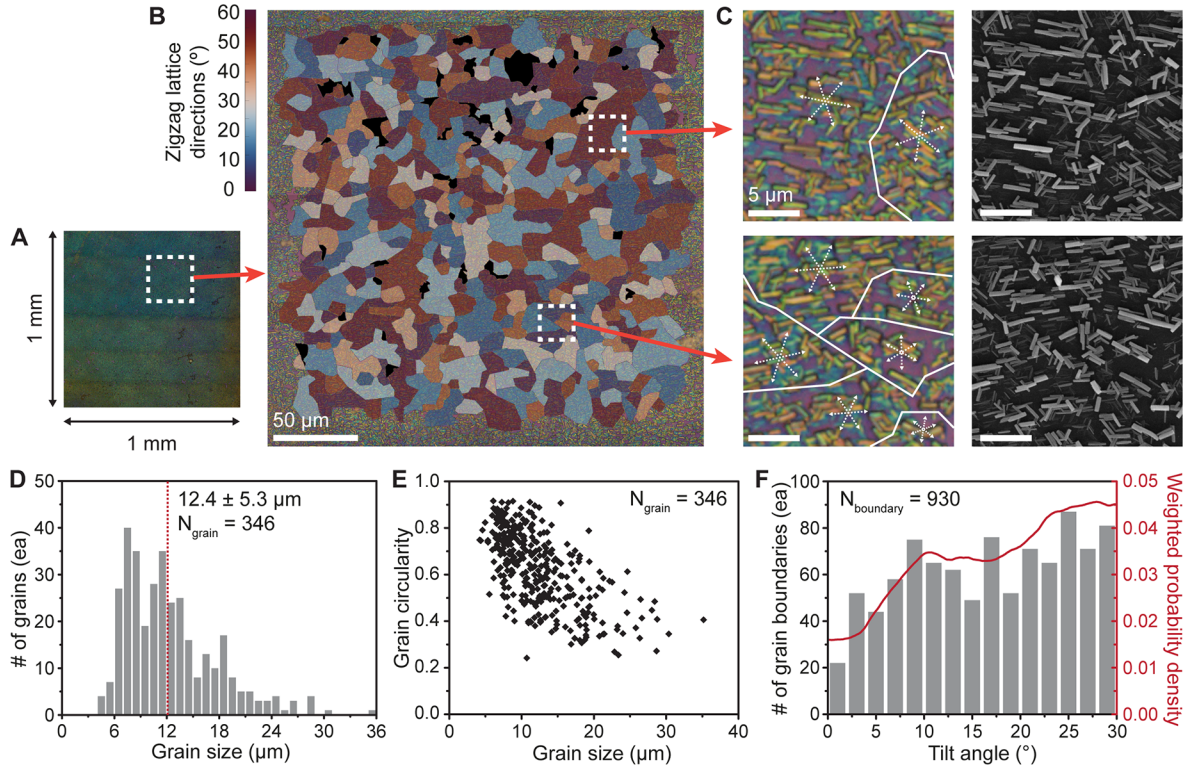

Figure 3. Large-area identification of crystal structures in single-layered polycrystalline graphene based on conventional optical microscopy of spin-coated AgCN microwires. (A) 1 × 1 mm^2 graphene sample on which epitaxial AgCN microwires are uniformly synthesized. (B) Crystal orientation map of polycrystalline graphene in (A). The optical microscopic image is shown with an overlay of a colormap indicating zigzag lattice orientations of the underlying grains. (C) Optical and SEM images from the square areas in (B). (D) Histogram of grain sizes, which are defined as square roots of grain areas. The average size and standard deviation of 346 grains are 12.4 μm ± 5.3 μm. (E) Scatter plot showing correlation between circularities and sizes of grains. (F) Histogram (gray bar) and weighted probability density function (red line, weighting factor: boundary lengths) of tilt angles between neighboring grains measured from 930 grain boundaries.

interactions of the 1D cyanide chains to hexagonal lattices.[36,37] Energetically favorable locations for metal cyanide adsorption onto 2D materials are hexagonally arranged, and because of this hexagonal arrangement, energetically favorable orientations of a straight molecular chain are along zigzag lattice directions of 2D materials (see Figure S12 for details).[36] Therefore, microwire axial directions, which are 1D chain directions of AgCN, are preferentially oriented along zigzag lattice directions of the underlying 2D materials.

Epitaxial AgCN Microwires for Visualizing Crystal Structures of 2D Materials. From the epitaxial AgCN microwires observable with conventional optical microscopy, one can come up with an idea to use the microwire directions as visualization markers of crystal structures (crystallographic orientations and grain boundaries) of underlying 2D materials. For metal cyanide nanomaterials, this idea has been suggested and experimentally verified with scanning electron microscopy (SEM) of AuCN nanowires[19,32] and optical microscopy of AgCN microwires.[35−37] While these previous works were limited to provide a proof-of-concept in small areas due to nonuniform and sparse growth characteristics, the spin-coating method in this study further improves reliability and practicality of the crystallographic identification. First, we quantitatively evaluate how precisely crystal orientations of 2D materials can be measured from optical images of the spin-coated AgCN microwires. Figure 2A shows an optical microscopic image of AgCN microwires spin coated on two grains of multilayered graphene separated by a wrinkle. The microwire orientations with the 3-fold symmetry are expected to indicate zigzag lattice orientations of the graphene grains. In the previous studies,[19,32,35−37] the crystallographic identification is performed with manually measuring the orientations of many individual wires. Dense and well-ordered growth of microwires in this study simplifies the analysis protocol based on 2D fast Fourier transform (FFT). Figure 2B clearly shows six-pointed asterisk (*) patterns in 2D FFT images of the two grains in Figure 2A, and the six bright lines indicate armchair lattice directions of the underlying graphene (the orientations orthogonal to microwire axial directions). Therefore, averaged radial intensities (Figure 2C and D) obtained from the FFT images enable us to estimate armchair lattice directions of the grains 1 and 2 (24.9° and 27.5°, respectively). The precision of this estimation can be evaluated with reference values of the armchair lattice directions (25.1° ± 0.2° and 27.5° ± 0.2°, respectively). These values are measured from SAED (selected area electron diffraction; Figure 2F) patterns of the graphene sample, which is transferred onto a TEM (transmission electron microscopy) grid after dissolving AgCN microwires (Figure 2E). We note that the measurement precision in this reference SAED analysis is estimated as ∼0.2° (Figure S13). The above results show that the present optical identification method has small measurement errors of 0.2° ± 0.2° and 0.0° ± 0.2° for grains 1 and 2, respectively. Additional graphene samples are also analyzed as shown in Table S1, presenting that the arithmetic mean and standard deviation of measurement errors for seven graphene samples are 0.48° ± 0.56°. The identical method can be applied for optically measuring armchair lattice directions of MoS_2 (Figure 2G) and hBN

https://doi.org/10.1021/acsnano.2c06963
ACS Nano 2022, 16, 20521−20532

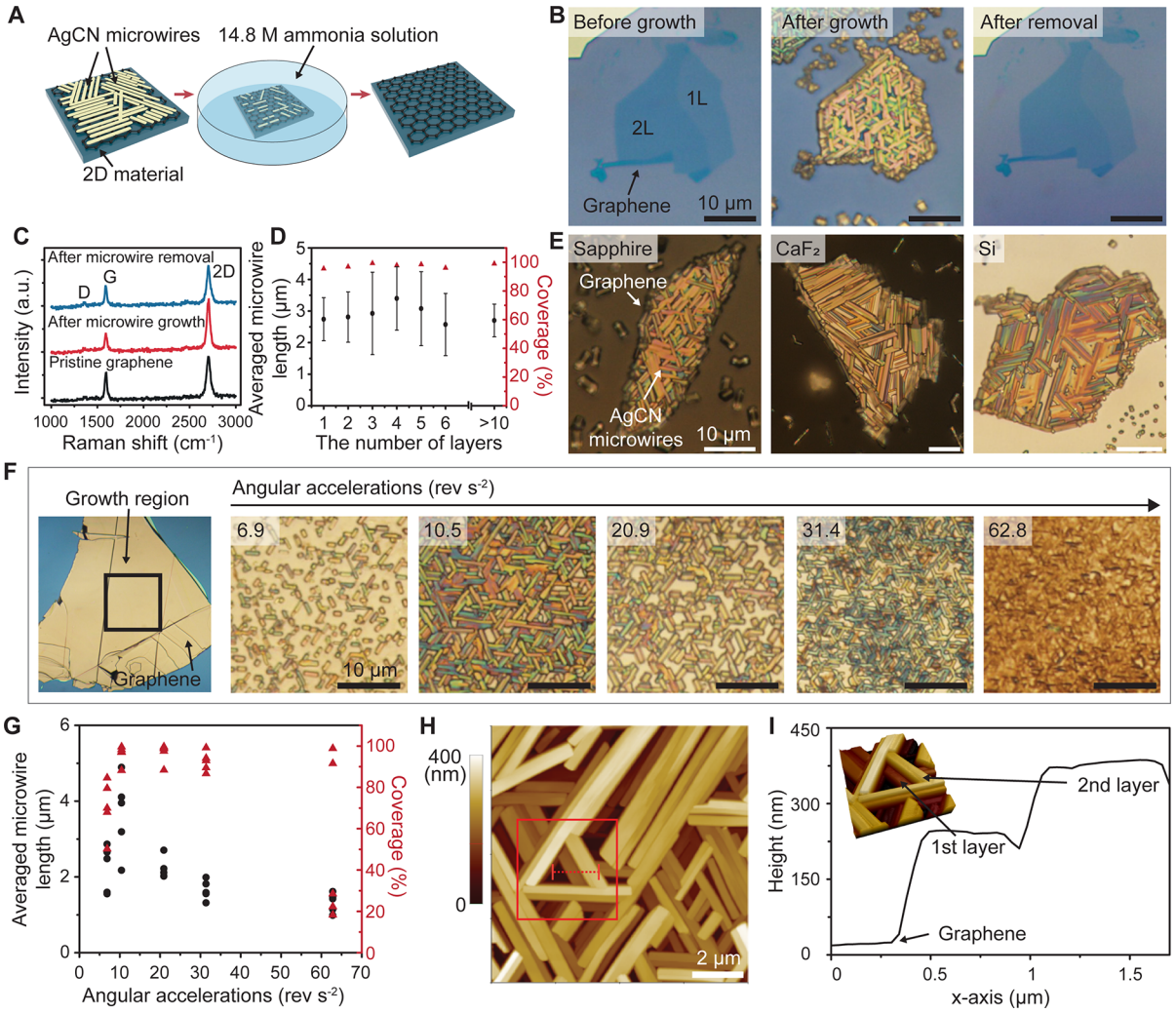

Figure 4. Removal and growth characteristics of AgCN microwires. (A) Schematic of the removal process using a simple wet chemistry. (B) Optical images of a graphene sample before growth, after growth, and after removal of AgCN microwires. The graphene sample contains single- and double- layered areas. (C) Raman spectra of pristine graphene (black), after microwire growth (red), and after microwire removal (blue). (D) Average lengths and coverages of AgCN microwires on graphene as a function of the number of graphene layers. (E) Optical images of spin-coated microwires on graphene supported on three different substrates (sapphire, CaF_2, and Si after native oxide removal). (F) Microwire growth characteristics depending on angular accelerations (rev/s^2) of the spin-coating process. (G) Average lengths and coverages of AgCN microwires on graphene as a function of angular accelerations. (H) AFM image of AgCN microwires on graphene. (I) Height profile along the dashed line in (H). The inset shows a 3D AFM image of the red square area in (H).

(Figure 2H), whose measurement errors are estimated as 0.6° ± 0.2° and 0.6° ± 0.2°, respectively. We would note that the epitaxial alignment of AgCN microwires was also confirmed on WS_2, WSe_2, $MoSe_2$, 2H-$MoTe_2$, 1T′-$MoTe_2$, Td-WTe_2, and 1T′-ReS_2.[36,37] Taken together, optical observations of spin-coated AgCN microwires can precisely measure crystal orientations of various 2D materials.

Crystallographic Mapping of Large-Area Graphene Using Spin-Coated Microwires. The present spin-coating method enables the large-scale optical identification of crystal structures in 2D materials because of the uniform and dense growth characteristics on a large area of 2D materials. We verify these abilities using single-layered polycrystalline graphene that is synthesized by CVD (chemical vapor deposition) and then transferred onto a SiO_2/Si substrate. Figure 3 shows a typical example for the large-scale identification, and two additional examples are presented in Figures S14 and S15. Uniform and dense growth of epitaxial AgCN microwires is experimentally confirmed on millimeter-scale graphene areas, as shown in a ∼1 mm by ∼1 mm area of a graphene sample on which AgCN microwires are spin coated (Figure 3A; Figure S1C). Cross validation of optical microscopic and SEM images captured in multiple areas (Figure 3C; Figure S16) demonstrates that AgCN microwires retain their 3-fold symmetric orientations and uniform areal densities. As shown in the previous paragraph, the microwire axial directions represent zigzag lattice directions of the underlying graphene directly, and the changes in the microwire directions also indicate tilt grain boundaries in the polycrystalline graphene. Therefore, a large-scale map of grain orientations (Figure 3B) can be obtained from simply analyzing the optical microscopic image with an in-house Matlab code based on 2D FFT. In the grain orientation map, zigzag lattice directions of 346 individual grains are indicated in the polycrystalline graphene area of ∼250 μm by ∼250 μm, and these grains form 930 grain boundaries with each other. The statistical analysis from the map shows that the grain sizes, defined as square roots of grain areas, have an average value of

https://doi.org/10.1021/acsnano.2c06963
ACS Nano 2022, 16, 20521−20532

12.4 μm ± 5.3 μm (Figure 3D). This size is much smaller than the average grain size (110 μm ± 10%) presented in the specification table[44] of the commercial "large grain" graphene we use here, while our method can overestimate (is very unlikely to underestimate) grain sizes. We additionally check two grain maps containing 204 grains (Figure S14B) and 310 grains (Figure S15B) by analyzing two different areas of the identical graphene sample and confirm that their grain sizes are also significantly smaller than the specification (14.2 ± 8.5 μm in Figure S14D and 12.4 ± 5.1 μm in Figure S15D). This unsatisfied specification found in the commercially purchased graphene means that monitoring processes such as the grain identification are mandatory for manufacturing commercial products from 2D materials. We also analyze statistical relationships between grain sizes and shapes (Figure 3E): Small grains show high probabilities to have convex areas (circularities $\approx$ 1), while large grains tend to have irregular shapes (circularities $\ll$ 1). Figure 3F shows a histogram of the misorientation angles of grain boundaries between adjacent grains and also shows a probability density function obtained from the histogram by adding grain lengths as a weighting factor. These two statistical analyses about grain boundaries show low frequencies (or low probabilities) in small misorientation angles (<~5°), which should be an artifact of the present identification method. The present method based on orientational changes in microwires cannot easily detect a grain boundary whose misorientation angle is small, and two constituent grains can be misidentified as a single grain. A solution to overcome this limit might be combining the present method with previous methods suggesting the direct decoration and identification of grain boundaries.[45−47] We also note that the present spin-coating method works successfully on a ~1 cm by ~1 cm area of a graphene sample (Figure S1C), which is achieved with manual dropping of the solution and spinning of the preheated substrate. Uniform microwire growth in a larger area such as a wafer scale might be possible with spray loading of the solution and spinning with in situ heating. Once the uniform growth in a larger area is achieved, it is straightforward to generate a grain orientation map that offers various statistical analyses (Figure 3D, E, and F; Figure S17). Therefore, our results show great potential for investigating as well as monitoring statistics in crystallographic properties of grains in a large area of 2D materials.

The above results experimentally verify that the present method provides an engineering tool to monitor crystallographic information (crystal orientations and grain boundaries) in a "large area" of 2D materials supported on a "SiO_2/Si substrate" using conventional optical microscopy. In addition, whether this monitoring method is "nondestructive" is important for engineering applications.[3] We therefore confirm that AgCN microwires can be easily etched out from graphene substrates using an aqueous ammonia solution (Figure 4A and B). The Raman spectra of graphene before and after microwire etching maintain very low D peaks (Figure 4C), confirming that measurable defects are not generated in the underlying graphene during the removal process (as well as the synthesis process) of AgCN microwires. This simple removal is an important factor as marker materials for the nondestructive monitoring process. Therefore, we can verify that the present method is an advanced tool for the crystallographic identification of 2D materials, compared to previous methods including TEM,[48−50] STM (scanning tunneling microscopy),[51] LEED (low-energy electron diffraction),[51−53] POM (polarized optical microscopy) of liquid crystals,[54−57] spectroscopic approaches based on nonlinear optical properties,[58−63] and direct imaging of epitaxial materials[15,16,19,32,35−37,64−68] (see Table S2 for details). For example, TEM[48−50] and LEED[51−53] are suitable only for conductive or ultrathin substrates, POM of liquid crystals cannot measure absolute crystallographic orientations,[54−57] and many epitaxial materials cannot be easily removed.[15,16,68] One can be concerned that crystallographic identification might become unnecessary because of the recent progress on wafer-scale synthesis of single-crystalline 2D materials. However, wafer-scale single crystals can be synthesized with limited types of 2D materials such as graphene, hBN, and MoS_2.[52,69] Wrinkles of 2D materials are also a main source for disturbing crystallographic control, but wrinkle-minimized synthesis[52] and transfer[70] methods are achieved only for graphene. Even if we assume that the above technologies are fully realized in a laboratory scale in the future, mass production on an industrial scale still needs monitoring processes for quality control.[71] The present method, therefore, has a potential to be a step of engineering procedures of 2D material device fabrication, because it shows nondestructive monitoring of crystal structures in a large area of 2D materials on a SiO_2/Si substrate.

Effects of Microwire Growth Conditions. We also investigate detailed effects of spin-coating conditions on growth characteristics of the AgCN microwires. First, the number of graphene layers on the SiO_2/Si substrate does not affect the microwire growth characteristics. Noticeable changes are not observed in lengths, coverages, and epitaxial alignments of the AgCN microwires spin-coated on single- and few-layered graphene (the number of graphene layers: 1−6 and >10), as shown in Figure 4B and D and Figures S18 and S19. This independency may be an unusual phenomenon because growth characteristics of inorganic materials are generally dependent on the number of graphene layers[9−11] and, in an extreme case, remote epitaxy is possible through single-layered graphene.[72] In these previous cases,[9−11,72] the substrates below graphene still interact with the epilayers as in the case of wetting transparency of graphene.[73−75] However, the system in our study shows that the van der Waals potential of graphene to AgCN seems strong enough to screen the potential field of underlying SiO_2. In addition, the observed independency explains the consistency of our growth results, which are obtained using two different types of graphene, multilayered graphene mechanically exfoliated from graphite (experimental results in Figures 1 and 2) and single-layered graphene synthesized by CVD (experimental results in Figure 3). Second, we test several different examples of substrate materials (sapphire, CaF_2, and Si), and the microwire growth characteristics are consistent on graphene supported on these substrates. The substrate mainly used in this study is a 300 nm SiO_2 layer on a Si (100) wafer, which is the most common substrate for 2D materials. The three substrates have different surface characteristics compared to SiO_2: Sapphire is a highly crystalline substrate, CaF_2 is an ionic substrate, and Si after native oxide removal is relatively hydrophobic. Optical images of spin-coated microwires (Figure 4E) do not show any noticeable differences from the SiO_2 case and between each other. This consistency may be because the ethanol-mixed solvent used in this study has relatively high affinities to all four of the substrates (although the affinities of aqueous solutions to the substrates are largely diverse), as indicated in Figure S20. Third, rotational acceleration of the spin-coating process

https://doi.org/10.1021/acsnano.2c06963
ACS Nano 2022, 16, 20521−20532

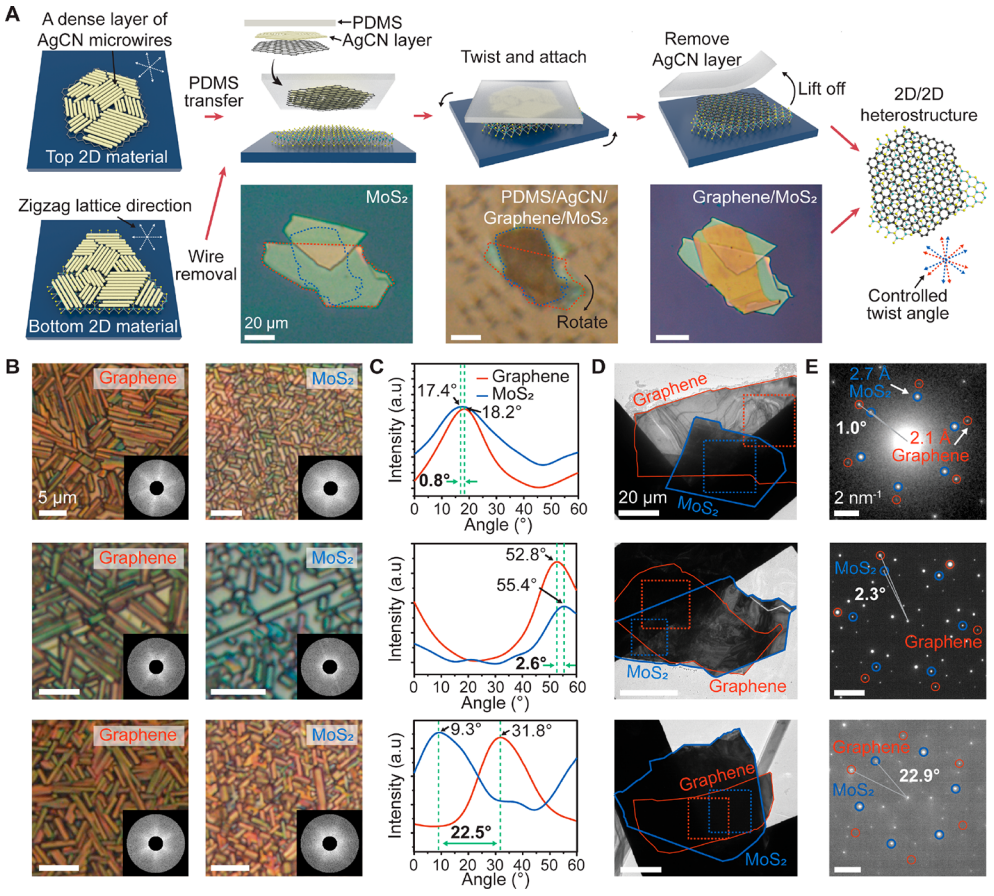

Figure 5. Fabrication of graphene-MoS_2 heterostructures with controlled twist angles. (A) Schematic views and corresponding optical images showing the heterostructure fabrication process. Spin-coated epitaxial microwires are used for controlling crystal orientations of 2D materials as well as providing a sacrificial layer in the 2D material transfer. (B to E) Graphene-MoS_2 heterostructures with three different targets of twist angles: 0° (top row), 3° (middle row), and 23° (bottom row). Optical images of epitaxial AgCN microwires on graphene and MoS_2 (B) indicate armchair lattice directions (insets: FFT of the images in (B)), which are measured from radial pixel intensities (C) of the FFT images. For experimental verifications, the fabricated graphene-MoS_2 heterostructures are transferred onto TEM grids (D), and twist angles are measured from SAED patterns (E).

strongly affects lengths and coverages of the AgCN microwires (Figure 4F and G). Interestingly, it is hard to find stable effects from rotational speed and time (Figure S21), while these two conditions are generally assumed important to control spin coating processes. It is because the AgCN microwire growth via solvent evaporation is done in the first few seconds of the spin-coating process, during which rotational acceleration governs centrifugal forces. The rotational acceleration of 10.5−20.9 rev/s^2 gives optimal lengths and coverages of the microwires (Figure 4G); thus we use this condition in our study. In addition, we test the effects of ethanol content in the precursor solution (Figure S10) and use the ethanol content of 60−70% in the spin-coating process. The spin-coating conditions discussed in this paragraph are used to synthesize AgCN microwires in our study, and we show vertical geometries of the synthesized microwires observed with AFM (atomic force microscopy) in Figure 4H and I. The microwires seem to have multiply stacked structures (usually, two layers): The thicknesses of the first and second layers are observed as ∼250 nm and ∼150 nm, respectively. The heights in AFM measurements can be correlated with the pixel colors in microscopic images; thus we might be able to further improve the precision of crystal orientation measurements using a color-based analysis of microscopic images (Figure S22).

Fabrication of van der Waals Heterostructures with Controlled Twist Angles. We apply our method to the fabrication of van der Waals heterostructures that present desired twist angles between vertically stacked 2D materials. Dense layers of epitaxial AgCN microwires obtained by our method serve as not only visualization markers for controlling the crystallographic orientations but also sacrificial layers for minimizing polymer residues in the 2D material transfer. Van der Waals heterostructures have received significant interest due to their unique physical properties and advanced functionalities.[1,2,12,76] In particular, the twist angle between 2D materials constitutes a critical parameter in manipulating electrical band structures of van der Waals heterostructures,[76,77] but it is still challenging to reliably control the twist angle as a desired value.[76] The present fabrication process (Figure 5A) solves this problem by including spin-coating steps of AgCN microwires on top and bottom 2D materials for optically visualizing crystallographic orientations. The densely coated microwires are also used as an interlayer between polymers such as PMMA (poly(methyl methacrylate)) and 2D materials and then are etched out during the transfer process. Therefore, we can prevent direct contact between the two

https://doi.org/10.1021/acsnano.2c06963
ACS Nano 2022, 16, 20521−20532

materials to minimize polymer residues that are one of the major concerns in the fabrication of van der Waals heterostructures.[78] This is why we can use a sticky PDMS (polydimethylsiloxane) layer whose component proportion is adjusted (prepolymer:cross-linker = 30:1) in our transfer step of 2D materials (Figures S23 and S24 and Movie S1). As shown in microscopic images in Figure 5A, we fabricate examples of van der Waals heterostructures using graphene and MoS_2 layers. Vertical stacking of the two materials is confirmed with Raman spectroscopic analyses (Figure S25), which are based on E^1_{2g} and A_{1g} peaks of MoS_2 and G peaks of graphene. The fabricated heterostructures of graphene and MoS_2 have three different target values of twist angles (0°, 3°, and 23°). Epitaxial AgCN microwires synthesized on graphene and MoS_2 (Figure 5B) indicate armchair lattice directions (insets of Figure 5B), thus enabling us to finely control crystallographic orientations of the two layers during the stacking process. The optical identification method indicates that the fabricated van der Waals heterostructures respectively have twist angles of 0.2°, 2.6°, and 22.5°, which are slightly different from the target angles due to motional errors of microstages. To measure reference values of twist angles, we transfer the fabricated van der Waals heterostructures onto TEM grids (Figure 5D) and observe SAED patterns of the heterostructures (Figure 5E). The twist angles are measured as 1.0°, 2.3°, and 22.9°, which respectively have differences of 1.0°, 0.7°, and 0.1° compared to the target twist angles. Although the previous studies[36,67] claimed that epitaxial markers enable us to achieve angular alignment accuracies of <0.1° or <0.2° (they claimed it using only a single example of the fabricated heterostructures), it would be fair to say that this method has the alignment accuracy of <∼1.0° when realized with laboratory-made tools and samples. By engineering optimizations of alignment stages and image analyses, this method can reliably achieve the ultrahigh alignment accuracy that the previous studies claimed. Adding the fact that various 2D materials (confirmed for graphene, MoS_2, hBN, WS_2, WSe_2, $MoSe_2$, 2H-$MoTe_2$, 1T′-$MoTe_2$, Td-WTe_2, and 1T′-ReS_2) allow the epitaxial alignment of AgCN microwires, we expect to realize a wide range of van der Waals heterostructures that have desired stacking sequences and crystal orientations.

CONCLUSION

In this study, we have shown that spin coating of AgCN dissolved in an aqueous ethanolic mixture can uniformly deposit a dense layer of epitaxial AgCN microwires onto various 2D materials including graphene, MoS_2, hBN, WS_2, and WSe_2. The aqueous ethanolic solution with controlled solvent properties facilitates uniform and conformal formation of the thin supersaturated solution layer during spin coating, which promotes heterogeneous crystal nucleation on 2D material surfaces over homogeneous nucleation in the bulk solution. Our experimental study confirms that spin-coated AgCN microwires are epitaxially aligned along zigzag lattice directions of 2D materials, grow to cover 98.5 ± 3.9% of the underlying graphene area, and can be simply etched out without degrading graphene's quality. Conventional optical microscopy of the spin-coated microwires enables large-area crystallographic mapping of grains in millimeter-sized polycrystalline graphene. We also have fabricated van der Waals heterostructures using the spin-coated microwires, which serve as not only visualization markers for controlling the crystallographic orientations (<∼1°) but also sacrificial layers for minimizing polymer residues in the 2D material transfer. In addition to these two practical applications, our study demonstrates the possibility of using 2D materials as templates for the epitaxial growth even with spin coating of inorganic crystals.

METHODS

Preparation of 2D Material Samples. A Si (100) wafer with a 300 nm SiO_2 layer is cleaned with acetone (99.8% purity, Daejung) and ethanol (99.9% purity, Daejung) for 10 min in an ultrasonic bath and rinsed with isopropyl alcohol (IPA, 99.5% purity, Sigma-Aldrich) and deionized (DI) water several times. The wafer is annealed at 200 °C for 2 h in the oven to remove any residual moisture. Graphene, MoS_2, hBN, WS_2, and WSe_2 flakes (purchased from NGS, graphene supermarket, and 2D semiconductors) are mechanically exfoliated on a 300 nm SiO_2/Si wafer using adhesive tape (Nitto, PVC). Single-layered large-grain CVD graphene on a 300 nm SiO_2/Si wafer (model: 920126, 4 in diameter, grain size: 110 μm × 110 μm ± 10%) was purchased from Sigma-Aldrich.[44] Sapphire and CaF_2 substrates (purchased from Green Optics and Edmund Optics) are cleaned with methanol and acetone in an ultrasonic bath for 10 min and then rinsed with IPA and DI water. A bare Si substrate is prepared by removing the native oxide layer in buffered oxide etch (BOE, Samchun).

AgCN Microwire Synthesis and Removal. Three different methods to synthesize AgCN microwires on 2D materials are described here: (i) Drop casting of an aqueous solution is a conventional approach used in the previous reports.[35−37] A AgCN aqueous solution is prepared by dissolving AgCN (13.3 mg, 2 mmol, 99% purity, Sigma-Aldrich) in an ammonia solution (50 mL, 14.8 M, Samchun). A 5 mL amount of an aqueous solution is dropped on the surface of 2D materials and dried at 150 °C on a hot plate for 10 min in air. (ii) Drop casting of an aqueous ethanol mixture uses a water−ethanol binary mixture. Typically, a saturated AgCN aqueous solution, which is made by dissolving AgCN in ammonia solution (10 mL, 14.8 M) until no additional AgCN is dissolved at room temperature, is added to ethanol at different ethanol volumetric ratios of 60−70%. After vigorous stirring for 2 min, 5 mL of an aqueous ethanol mixture is dropped on the surface of 2D materials and dried at 150 °C on a hot plate for 10 min in air. (iii) Spin coating of an aqueous ethanol mixture combines the above binary mixture and a spin-coating process. In a typical procedure, SiO_2/Si substrates on which various 2D materials are placed are adhered onto an aluminum plate. After heating the plate at 150 °C for 5 min, the hot substrates are quickly loaded on a spin coater (ACE-200, DongAh). A 10−30 mL amount of an aqueous ethanol mixture is dropped and then is spun at 2000−3000 rpm for 10 s with the rotational acceleration of 10.5−20.9 rev/s^2. The detailed parameters for spin coating are described in Table S3. Due to the high solubility of AgCN in ammonia solution, AgCN microwires are etched out by immersing the sample in an ammonia solution for 5 min at room temperature. The etching time and temperature can be increased up to ∼2 h and ∼80 °C, respectively, if there is an additional concern about clean surfaces. Then, the sample is rinsed 2 or 3 times in DI water for 5 min.

Fabrication of Van der Waals Heterostructures. For the fabrication of graphene-MoS_2 heterostructures, a sticky PDMS stamp is prepared by drop casting of 30:1 (weight ratio, prepolymer to cross-linker) PDMS resin onto a glass slide. In a typical curing procedure at 80 °C for 30 min, a hemispherical PDMS stamp is naturally formed by suspending the glass slide upside down on a Petri dish (Figure S24). Next, AgCN microwires are spin coated on graphene and MoS_2 samples prepared on SiO_2 wafers. After measuring crystal orientations using the spin-coated microwires, the microwires on MoS_2 are clearly removed by the wet-etching procedure. Thereafter, graphene and spin-coated microwires are transferred onto the as-prepared PDMS stamp using laboratory-made tools (Figure S23; Movie S1). Note that sandwiched microwires between graphene and the PDMS stamp act as sacrificial layers, preventing the direct contacts between the graphene and the polymer. In an angular alignment procedure, the

https://doi.org/10.1021/acsnano.2c06963
ACS Nano 2022, 16, 20521−20532

bottom MoS_2 and top graphene layers are twisted depending on premeasured crystal orientations. The bottom MoS_2 layer is lifted and attached onto the top graphene layer. After a baking process at 80 °C for 30 min to enhance the adhesion between graphene and MoS_2, the AgCN microwires are dissolved in an ammonia solution while the PDMS stamp is gradually separated. The graphene-MoS_2 heterostructure is rinsed in DI water several times and dried in air.

TEM Sample Preparation. Two-dimensional materials on TEM grids (Au 200 mesh, EMS) are prepared using the PMMA-assisted transfer method. In detail, a PMMA layer is spin coated (500 rpm, 30 s) on 2D materials placed on a SiO_2/Si substrate and is sequentially heated at 80 °C for 5 min and at 120 °C for 20 min. The edge of the PMMA film is scratched by a sharp tip tweezer, and then the PMMA-coated substrate is ultrasonicated for 5 min in DI water to exfoliate the PMMA layer from the SiO_2/Si substrate. Then, TEM grids are attached on the 2D materials side of the PMMA layer, and 2D materials are transferred by removing the PMMA layer in acetone for 1 h.

Characterization and Data Presentation. The cyclic colormap of vikO[79] is used for the crystal orientation maps in Figure 3B, Figure S14B, and Figure S15B, in which two angles differing by 60° indicate the same crystal orientations due to the hexagonal symmetry of graphene. Atomic configurations of epitaxial AgCN crystals on graphene are generated using the software VESTA.[80] TEM images are captured using a JEOL 2100F TEM operated at 200 kV. Optical microscopy (BX53M, Olympus) and field emission scanning electron microscopy (FE-SEM) (MIRA3, TESCAN) are used to capture microscopic images of AgCN microwires. The height profile of spin-coated AgCN microwires is obtained using AFM (XE-100, Park Systems), and Raman spectra are acquired using a LabRAM ARAMIS Raman microscope with a 532 nm excitation wavelength.

ASSOCIATED CONTENT

Supporting Information

The Supporting Information is available free of charge at https://pubs.acs.org/doi/10.1021/acsnano.2c06963.

Supporting figures (Figures S1−S25) and supporting tables (Tables S1−S3) showing optical microscopy, SEM, TEM, AFM, Raman spectroscopy, growth conditions, etc., of epitaxial AgCN microwires spin-coated on various 2D materials (PDF)

Movie S1: Optical microscopic movie showing the graphene transfer process with the PDMS stamp presented in Figure S23; the movie plays in 2 times faster than real time (MP4)

AUTHOR INFORMATION

Corresponding Author

Won Chul Lee − *Department of Mechanical Engineering, BK21FOUR ERICA-ACE Center, Hanyang University, Ansan, Gyeonggi 15588, Republic of Korea;* orcid.org/0000-0001-8479-0836; Email: wonchullee@hanyang.ac.kr

Authors

Jimin Ham − *Department of Mechanical Engineering, BK21FOUR ERICA-ACE Center, Hanyang University, Ansan, Gyeonggi 15588, Republic of Korea*

Jaemook Lim − *Department of Mechanical Engineering, BK21FOUR ERICA-ACE Center, Hanyang University, Ansan, Gyeonggi 15588, Republic of Korea*

Sukjoon Hong − *Department of Mechanical Engineering, BK21FOUR ERICA-ACE Center, Hanyang University, Ansan, Gyeonggi 15588, Republic of Korea;* orcid.org/0000-0002-5988-4600

Complete contact information is available at: https://pubs.acs.org/10.1021/acsnano.2c06963

Author Contributions

J.H. and W.C.L. conceived the design of the research. S.H. and W.C.L. supervised the project. J.H. and J.L. performed the experimental study. J.H. and W.C.L. analyzed the data. J.H., S.H., and W.C.L. wrote the manuscript.

Notes

The authors declare no competing financial interest.

ACKNOWLEDGMENTS

This work was supported by the National Research Foundation of Korea (NRF) grant funded by the Korea government (MSIT) (No. 2022R1A4A3031263 and No. 2021R1A2C1011797).

REFERENCES

(1) Novoselov, K. S.; Mishchenko, A.; Carvalho, A.; Castro Neto, A. H. 2D materials and Van Der Waals Heterostructures. *Science* **2016**, *353*, aac9439.

(2) Jariwala, D.; Marks, T. J.; Hersam, M. C. Mixed-Dimensional Van Der Waals Heterostructures. *Nat. Mater.* **2017**, *16*, 170−181.

(3) Yang, J.; Kim, K.; Lee, Y.; Kim, K.; Lee, W. C.; Park, J. Self-Organized Growth and Self-Assembly of Nanostructures on 2D Materials. *FlatChem.* **2017**, *5*, 50−68.

(4) Hong, G.; Wu, Q.-H.; Ren, J.; Wang, C.; Zhang, W.; Lee, S.-T. Recent Progress in Organic Molecule/Graphene Interfaces. *Nano Today* **2013**, *8*, 388−402.

(5) Ohring, M. In *Materials Science of Thin Films*, second ed.; Ohring, M., Ed.; Academic Press: Cambridge, 2002; Chapter 8, pp 417−494.

(6) Kum, H.; Lee, D.; Kong, W.; Kim, H.; Park, Y.; Kim, Y.; Baek, Y.; Bae, S.-H.; Lee, K.; Kim, J. Epitaxial Growth and Layer-Transfer Techniques for Heterogeneous Integration of Materials for Electronic and Photonic Devices. *Nat. Electron.* **2019**, *2*, 439−450.

(7) Kelso, M. V.; Mahenderkar, N. K.; Chen, Q.; Tubbesing, J. Z.; Switzer, J. A. Spin Coating Epitaxial Films. *Science* **2019**, *364*, 166−169.

(8) Koma, A. Van Der Waals Epitaxy—a New Epitaxial Growth Method for a Highly Lattice-Mismatched System. *Thin Solid Films* **1992**, *216*, 72−76.

(9) Hong, Y. J.; Fukui, T. Controlled Van Der Waals Heteroepitaxy of InAs Nanowires on Carbon Honeycomb Lattices. *ACS Nano* **2011**, *5*, 7576−7584.

(10) Hong, Y. J.; Lee, W. H.; Wu, Y.; Ruoff, R. S.; Fukui, T. Van Der Waals Epitaxy of InAs Nanowires Vertically Aligned on Single-Layer Graphene. *Nano Lett.* **2012**, *12*, 1431−1436.

(11) Zhou, H.; Yu, F.; Chen, M.; Qiu, C.; Yang, H.; Wang, G.; Yu, T.; Sun, L. The Transformation of a Gold Film on Few-Layer Graphene to Produce Either Hexagonal or Triangular Nanoparticles during Annealing. *Carbon* **2013**, *52*, 379−387.

(12) Zhou, X.; Yu, G. Preparation Engineering of Two-Dimensional Heterostructures via Bottom-Up Growth for Device Applications. *ACS Nano* **2021**, *15*, 11040−11065.

(13) Gong, Y.; Lin, J.; Wang, X.; Shi, G.; Lei, S.; Lin, Z.; Zou, X.; Ye, G.; Vajtai, R.; Yakobson, B. I.; Terrones, H.; Terrones, M.; Tay; Beng, K.; Lou, J.; Pantelides, S. T.; Liu, Z.; Zhou, W.; Ajayan, P. M. Vertical and In-Plane Heterostructures from WS_2/MoS_2 Monolayers. *Nat. Mater.* **2014**, *13*, 1135−1142.

(14) Shi, Y.; Zhou, W.; Lu, A.-Y.; Fang, W.; Lee, Y.-H.; Hsu, A. L.; Kim, S. M.; Kim, K. K.; Yang, H. Y.; Li, L.-J.; Idrobo, J.-C.; Kong, J. Van Der Waals Epitaxy of MoS_2 Layers Using Graphene As Growth Templates. *Nano Lett.* **2012**, *12*, 2784−2791.

(15) Ago, H.; Fukamachi, S.; Endo, H.; Solís-Fernández, P.; Mohamad Yunus, R.; Uchida, Y.; Panchal, V.; Kazakova, O.; Tsuji, M. Visualization of Grain Structure and Boundaries of Polycrystalline

Graphene and Two-Dimensional Materials by Epitaxial Growth of Transition Metal Dichalcogenides. *ACS Nano* **2016**, *10*, 3233−3240.
(16) Kim, S. J.; Luo, D.; Park, K.; Choe, M.; Kim, D. W.; Wang, M.; Jung, W.-B.; Lee, Z.; Ruoff, R. S.; Jung, H.-T. Mapping Graphene Grain Orientation by the Growth of WS_2 Films with Oriented Cracks. *Chem. Mater.* **2020**, *32*, 7484−7491.
(17) Huang, X.; Zeng, Z.; Bao, S.; Wang, M.; Qi, X.; Fan, Z.; Zhang, H. Solution-Phase Epitaxial Growth of Noble Metal Nanostructures on Dispersible Single-Layer Molybdenum Disulfide Nanosheets. *Nat. Commun.* **2013**, *4*, 1444.
(18) Schornbaum, J.; Winter, B.; Schießl, S. P.; Gannott, F.; Katsukis, G.; Guldi, D. M.; Spiecker, E.; Zaumseil, J. Epitaxial Growth of PbSe Quantum Dots on MoS_2 Nanosheets and Their Near-Infrared Photoresponse. *Adv. Funct. Mater.* **2014**, *24*, 5798−5806.
(19) Lee, W. C.; Kim, K.; Park, J.; Koo, J.; Jeong, H. Y.; Lee, H.; Weitz, D. A.; Zettl, A.; Takeuchi, S. Graphene-Templated Directional Growth of an Inorganic Nanowire. *Nat. Nanotechnol.* **2015**, *10*, 423−428.
(20) Lin, Z.; Yin, A.; Mao, J.; Xia, Y.; Kempf, N.; He, Q.; Wang, Y.; Chen, C.-Y.; Zhang, Y.; Ozolins, V.; Ren, Z.; Huang, Y.; Duan, X. Scalable Solution-Phase Epitaxial Growth of Symmetry-Mismatched Heterostructures on Two-Dimensional Crystal Soft Template. *Sci. Adv.* **2016**, *2*, e1600993.
(21) Zhang, Z.; Sun, F.; Zhu, Z.; Dai, J.; Gao, K.; Wei, Q.; Shi, X.; Sun, Q.; Yan, Y.; Li, H.; Yu, H.; Xing, G.; Huang, X.; Huang, W. Unconventional Solution-Phase Epitaxial Growth of Organic-Inorganic Hybrid Perovskite Nanocrystals on Metal Sulfide Nanosheets. *Sci. China Mater.* **2019**, *62*, 43−53.
(22) Gao, X.; Zhu, Y.; Yi, D.; Zhou, J.; Zhang, S.; Yin, C.; Ding, F.; Zhang, S.; Yi, X.; Wang, J.; Tong, L.; Han, Y.; Liu, Z.; Zhang, J. Ultrathin Graphdiyne Film on Graphene Through Solution-Phase Van Der Waals Epitaxy. *Sci. Adv.* **2018**, *4*, eaat6378.
(23) Huang, X.; Qi, X.; Boey, F.; Zhang, H. Graphene-Based Composites. *Chem. Soc. Rev.* **2012**, *41*, 666−686.
(24) Diao, Y.; Shaw, L.; Bao, Z.; Mannsfeld, S. C. B. Morphology Control Strategies for Solution-Processed Organic Semiconductor Thin Films. *Energy Environ. Sci.* **2014**, *7*, 2145−2159.
(25) Jeon, N. J.; Noh, J. H.; Kim, Y. C.; Yang, W. S.; Ryu, S.; Seok, S. I. Solvent Engineering for High-Performance Inorganic−Organic Hybrid Perovskite Solar Cells. *Nat. Mater.* **2014**, *13*, 897−903.
(26) Nie, W.; Tsai, H.; Asadpour, R.; Blancon, J.-C.; Neukirch, A. J.; Gupta, G.; Crochet, J. J.; Chhowalla, M.; Tretiak, S.; Alam, M. A.; Wang, H.-L.; Mohite, A. D. High-Efficiency Solution-Processed Perovskite Solar Cells with Millimeter-Scale Grains. *Science* **2015**, *347*, 522−525.
(27) Tang, G.; You, P.; Tai, Q.; Yang, A.; Cao, J.; Zheng, F.; Zhou, Z.; Zhao, J.; Chan, P. K. L.; Yan, F. Solution-Phase Epitaxial Growth of Perovskite Films on 2D Material Flakes for High-Performance Solar Cells. *Adv. Mater.* **2019**, *31*, 1807689.
(28) Cao, J.; Tang, G.; You, P.; Wang, T.; Zheng, F.; Zhao, J.; Yan, F. Enhanced Performance of Planar Perovskite Solar Cells Induced by Van Der Waals Epitaxial Growth of Mixed Perovskite Films on WS_2 Flakes. *Adv. Funct. Mater.* **2020**, *30*, 2002358.
(29) Zhou, Q.; Duan, J.; Yang, X.; Duan, Y.; Tang, Q. Interfacial Strain Release from the $WS_2/CsPbBr_3$ Van Der Waals Heterostructure for 1.7 V Voltage All-Inorganic Perovskite Solar Cells. *Angew. Chem., Int. Ed.* **2020**, *59*, 21997−22001.
(30) Wang, T.; Zheng, F.; Tang, G.; Cao, J.; You, P.; Zhao, J.; Yan, F. 2D WSe_2 Flakes for Synergistic Modulation of Grain Growth and Charge Transfer in Tin-Based Perovskite Solar Cells. *Adv. Sci.* **2021**, *8*, 2004315.
(31) Kiriya, D.; Zhou, Y.; Nelson, C.; Hettick, M.; Madhvapathy, S. R.; Chen, K.; Zhao, P.; Tosun, M.; Minor, A. M.; Chrzan, D. C.; Javey, A. Oriented Growth of Gold Nanowires on MoS_2. *Adv. Funct. Mater.* **2015**, *25*, 6257−6264.
(32) Kim, J.; Lim, K.; Lee, Y.; Kim, J.; Kim, K.; Park, J.; Kim, K.; Lee, W. C. Precise Identification of Graphene's Crystal Structures by Removable Nanowire Epitaxy. *J. Phys. Chem. Lett.* **2017**, *8*, 1302−1309.
(33) Jang, J.; Lee, Y.; Yoon, J.-Y.; Yoon, H. H.; Koo, J.; Choe, J.; Jeon, S.; Sung, J.; Park, J.; Lee, W. C.; Lee, H.; Jeong, H. Y.; Park, K.; Kim, K. One-Dimensional Assembly on Two-Dimensions: AuCN Nanowire Epitaxy on Graphene for Hybrid Phototransistors. *Nano Lett.* **2018**, *18*, 6214−6221.
(34) Jeon, S.; Heo, T.; Hwang, S.-Y.; Ciston, J.; Bustillo, K. C.; Reed, B. W.; Ham, J.; Kang, S.; Kim, S.; Lim, J.; Lim, K.; Kim, J. S.; Kang, M.-H.; Bloom, R. S.; Hong, S.; Kim, K.; Zettl, A.; Kim, W. Y.; Ercius, P.; Park, J.; et al. Reversible Disorder-Order Transitions in Atomic Crystal Nucleation. *Science* **2021**, *371*, 498−503.
(35) Ham, J.; Lee, Y.; Kim, J.; Lim, K.; Lee, S.; Jeon, S.; Kim, K.; Lee, W. C.Facile Identification of Graphene's Crystal Orientations by Optical Microscopy of Self-Aligned Microwires. In *Micro Electro Mechanical Systems 2019, Proceedings of the 32nd IEEE International Conference on Micro Electro Mechanical Systems (MEMS)*, Seoul, Korea, January 27−31, 2019; Takeuchi, S., Yoon, J.-B., Eds.; IEEE: New York, USA, 2019; pp 264−265 DOI: 10.1109/MEMSYS.2019.8870631.
(36) Lee, Y.; Koo, J.; Lee, S.; Yoon, J.-Y.; Kim, K.; Jang, M.; Jang, J.; Choe, J.; Li, B.-W.; Le, C. T.; Ullah, F.; Kim, Y. S.; Hwang, J. Y.; Lee, W. C.; Ruoff, R. S.; Cheong, H.; Cheon, J.; Lee, H.; Kim, K. Universal Oriented Van Der Waals Epitaxy of 1D Cyanide Chains on Hexagonal 2D Crystals. *Adv. Sci.* **2020**, *7*, 1900757.
(37) Jang, M.; Bae, H.; Lee, Y.; Na, W.; Yu, B.; Choi, S.; Cheong, H.; Lee, H.; Kim, K. Unidirectional Alignment of AgCN Microwires on Distorted Transition Metal Dichalcogenide Crystals. *ACS Appl. Mater. Interfaces* **2021**, *13*, 8727−8735.
(38) Park, C.; Ham, J.; Heo, Y. J.; Lee, W. C.Epitaxial Growth of Diamond-Shaped $Au_{(1/2)}Ag_{(1/2)}CN$ Nanocrystals on Graphene.*Materials***2021**, *14*.
(39) Deegan, R. D.; Bakajin, O.; Dupont, T. F.; Huber, G.; Nagel, S. R.; Witten, T. A. Capillary Flow As the Cause of Ring Stains from Dried Liquid Drops. *Nature* **1997**, *389*, 827−829.
(40) Rawashdeh-Omary, M. A.; Omary, M. A.; Patterson, H. H. Oligomerization of $Au(CN)_2^-$ and $Ag(CN)_2^-$ Ions in Solution via Ground-State Aurophilic and Argentophilic Bonding. *J. Am. Chem. Soc.* **2000**, *122*, 10371−10380.
(41) Jia, Y. F.; Steele, C. J.; Hayward, I. P.; Thomas, K. M. Mechanism of Adsorption of Gold and Silver Species on Activated Carbons. *Carbon* **1998**, *36*, 1299−1308.
(42) Klauber, C. Acid Induced Oligomerization of Aurocyanide Adsorbed on Carbon. *Surf. Sci.* **1988**, *203*, 118−128.
(43) Chippindale, A. M.; Hibble, S. J.; Bilbé, E. J.; Marelli, E.; Hannon, A. C.; Allain, C.; Pansu, R.; Hartl, F. Mixed Copper, Silver, and Gold Cyanides, $(M_xM'_{1-x})CN$: Tailoring Chain Structures to Influence Physical Properties. *J. Am. Chem. Soc.* **2012**, *134*, 16387−16400.
(44) *Sigma-Aldrich Home Page on R2R Monolayer Large Grain CVD Graphene on Silicon Wafer*. https://www.sigmaaldrich.com/product/aldrich/920126 (accessed 2022−12−02).
(45) Duong, D. L.; Han, G. H.; Lee, S. M.; Gunes, F.; Kim, E. S.; Kim, S. T.; Kim, H.; Ta, Q. H.; So, K. P.; Yoon, S. J.; Chae, S. J.; Jo, Y. W.; Park, M. H.; Chae, S. H.; Lim, S. C.; Choi, J. Y.; Lee, Y. H. Probing Graphene Grain Boundaries with Optical Microscopy. *Nature* **2012**, *490*, 235−239.
(46) Kim, K.; Lee, H.-B.-R.; Johnson, R. W.; Tanskanen, J. T.; Liu, N.; Kim, M.-G.; Pang, C.; Ahn, C.; Bent, S. F.; Bao, Z. Selective Metal Deposition at Graphene Line Defects by Atomic Layer Deposition. *Nat. Commun.* **2014**, *5*, 4781.
(47) Wang, S.; Yu, Y.; Zhang, S.; Zhang, S.; Xu, H.; Zou, X.; Zhang, J. Atomic-Scale Studies of Overlapping Grain Boundaries between Parallel and Quasi-Parallel Grains in Low-Symmetry Monolayer ReS_2. *Matter* **2020**, *3*, 2108−2123.
(48) Huang, P. Y.; Ruiz-Vargas, C. S.; van der Zande, A. M.; Whitney, W. S.; Levendorf, M. P.; Kevek, J. W.; Garg, S.; Alden, J. S.; Hustedt, C. J.; Zhu, Y.; Park, J.; McEuen, P. L.; Muller, D. A. Grains and Grain Boundaries in Single-Layer Graphene Atomic Patchwork Quilts. *Nature* **2011**, *469*, 389−392.

(49) Kim, K.; Lee, Z.; Regan, W.; Kisielowski, C.; Crommie, M. F.; Zettl, A. Grain Boundary Mapping in Polycrystalline Graphene. *ACS Nano* **2011**, *5*, 2142−2146.
(50) Caplins, B. W.; Holm, J. D.; White, R. M.; Keller, R. R. Orientation Mapping of Graphene Using 4D STEM-in-SEM. *Ultramicroscopy* **2020**, *219*, 113137.
(51) Wintterlin, J.; Bocquet, M. L. Graphene on Metal Surfaces. *Surf. Sci.* **2009**, *603*, 1841−1852.
(52) Wang, M.; Huang, M.; Luo, D.; Li, Y.; Choe, M.; Seong, W. K.; Kim, M.; Jin, S.; Wang, M.; Chatterjee, S.; Kwon, Y.; Lee, Z.; Ruoff, R. S. Single-Crystal, Large-Area, Fold-Free Monolayer Graphene. *Nature* **2021**, *596*, 519−524.
(53) Zhao, W.; Xia, B.; Lin, L.; Xiao, X.; Liu, P.; Lin, X.; Peng, H.; Zhu, Y.; Yu, R.; Lei, P.; Wang, J.; Zhang, L.; Xu, Y.; Zhao, M.; Peng, L.; Li, Q.; Duan, W.; Liu, Z.; Fan, S.; Jiang, K. Low-Energy Transmission Electron Diffraction and Imaging of Large-Area Graphene. *Sci. Adv.* **2017**, *3*, e1603231.
(54) Kim, D. W.; Kim, Y. H.; Jeong, H. S.; Jung, H.-T. Direct Visualization of Large-Area Graphene Domains and Boundaries by Optical Birefringency. *Nat. Nanotechnol.* **2012**, *7*, 29−34.
(55) Son, J.-H.; Baeck, S.-J.; Park, M.-H.; Lee, J.-B.; Yang, C.-W.; Song, J.-K.; Zin, W.-C.; Ahn, J.-H. Detection of Graphene Domains and Defects Using Liquid Crystals. *Nat. Commun.* **2014**, *5*, 3484.
(56) Kim, D. W.; Ok, J. M.; Jung, W.-B.; Kim, J.-S.; Kim, S. J.; Choi, H. O.; Kim, Y. H.; Jung, H.-T. Direct Observation of Molybdenum Disulfide, MoS_2, Domains by Using a Liquid Crystalline Texture Method. *Nano Lett.* **2015**, *15*, 229−234.
(57) Shehzad, M. A.; Hussain, S.; Lee, J.; Jung, J.; Lee, N.; Kim, G.; Seo, Y. Study of Grains and Boundaries of Molybdenum Diselenide and Tungsten Diselenide Using Liquid Crystal. *Nano Lett.* **2017**, *17*, 1474−1481.
(58) Yin, X.; Ye, Z.; Chenet, D. A.; Ye, Y.; O'Brien, K.; Hone, J. C.; Zhang, X. Edge Nonlinear Optics on a MoS_2 Atomic Monolayer. *Science* **2014**, *344*, 488−490.
(59) Xia, F.; Wang, H.; Jia, Y. Rediscovering Black Phosphorus As an Anisotropic Layered Material for Optoelectronics and Electronics. *Nat. Commun.* **2014**, *5*, 4458.
(60) Chenet, D. A.; Aslan, O. B.; Huang, P. Y.; Fan, C.; van der Zande, A. M.; Heinz, T. F.; Hone, J. C. In-Plane Anisotropy in Mono- and Few-Layer ReS_2 Probed by Raman Spectroscopy and Scanning Transmission Electron Microscopy. *Nano Lett.* **2015**, *15*, 5667−5672.
(61) Chen, S.-Y.; Goldstein, T.; Venkataraman, D.; Ramasubramaniam, A.; Yan, J. Activation of New Raman Modes by Inversion Symmetry Breaking in Type II Weyl Semimetal Candidate T′-$MoTe_2$. *Nano Lett.* **2016**, *16*, 5852−5860.
(62) Ma, X.; Guo, P.; Yi, C.; Yu, Q.; Zhang, A.; Ji, J.; Tian, Y.; Jin, F.; Wang, Y.; Liu, K.; Xia, T.; Shi, Y.; Zhang, Q. Raman Scattering in The Transition-Metal Dichalcogenides of 1T′−$MoTe_2$, T_d−$MoTe_2$, and T_d−WTe_2. *Phys. Rev. B* **2016**, *94*, 214105.
(63) Choi, Y.; Kim, K.; Lim, S. Y.; Kim, J.; Park, J. M.; Kim, J. H.; Lee, Z.; Cheong, H. Complete Determination of the Crystallographic Orientation of ReX_2 (X = S, Se) by Polarized Raman Spectroscopy. *Nanoscale Horiz.* **2020**, *5*, 308−315.
(64) Prado, M. C.; Nascimento, R.; Moura, L. G.; Matos, M. J. S.; Mazzoni, M. S. C.; Cancado, L. G.; Chacham, H.; Neves, B. R. A. Two-Dimensional Molecular Crystals of Phosphonic Acids on Graphene. *ACS Nano* **2011**, *5*, 394−398.
(65) Prado, M. C.; Nascimento, R.; Faria, B. E.; Matos, M. J.; Chacham, H.; Neves, B. R. Nanometre-Scale Identification of Grain Boundaries in MoS_2 through Molecular Decoration. *Nanotechnology* **2015**, *26*, 475702.
(66) Wang, J.; Yu, H.; Zhou, X.; Liu, X.; Zhang, R.; Lu, Z.; Zheng, J.; Gu, L.; Liu, K.; Wang, D.; Jiao, L. Probing the Crystallographic Orientation of Two-Dimensional Atomic Crystals with Supramolecular Self-Assembly. *Nat. Commun.* **2017**, *8*, 377.
(67) Cui, X.; Sun, L.; Zeng, Y.; Hao, Y.; Liu, Y.; Wang, D.; Yi, Y.; Loh, K. P.; Zheng, J.; Liu, Y. Visualization of Crystallographic Orientation and Twist Angles in Two-Dimensional Crystals with an Optical Microscope. *Nano Lett.* **2020**, *20*, 6059−6066.
(68) Zhan, L.; Wan, W.; Zhu, Z.; Zhao, Z.; Zhang, Z.; Shih, T.-M.; Cai, W. A Visualization Method for Probing Grain Boundaries of Single Layer Graphene via Molecular Beam Epitaxy. *Nanotechnology* **2017**, *28*, 305601.
(69) Zhang, L.; Dong, J.; Ding, F. Strategies, Status, and Challenges in Wafer Scale Single Crystalline Two-Dimensional Materials Synthesis. *Chem. Rev.* **2021**, *121*, 6321−6372.
(70) Leong, W. S.; Wang, H.; Yeo, J.; Martin-Martinez, F. J.; Zubair, A.; Shen, P.-C.; Mao, Y.; Palacios, T.; Buehler, M. J.; Hong, J.-Y.; Kong, J. Paraffin-Enabled Graphene Transfer. *Nat. Commun.* **2019**, *10*, 867.
(71) Deng, B.; Liu, Z.; Peng, H. Toward Mass Production of CVD Graphene Films. *Adv. Mater.* **2019**, *31*, 1800996.
(72) Kim, Y.; Cruz, S. S.; Lee, K.; Alawode, B. O.; Choi, C.; Song, Y.; Johnson, J. M.; Heidelberger, C.; Kong, W.; Choi, S.; Qiao, K.; Almansouri, I.; Fitzgerald, E. A.; Kong, J.; Kolpak, A. M.; Hwang, J.; Kim, J. Remote Epitaxy through Graphene Enables Two-Dimensional Material-Based Layer Transfer. *Nature* **2017**, *544*, 340−343.
(73) Rafiee, J.; Mi, X.; Gullapalli, H.; Thomas, A. V.; Yavari, F.; Shi, Y.; Ajayan, P. M.; Koratkar, N. A. Wetting Transparency of Graphene. *Nat. Mater.* **2012**, *11*, 217−222.
(74) Shih, C.-J.; Strano, M. S.; Blankschtein, D. Wetting Translucency of Graphene. *Nat. Mater.* **2013**, *12*, 866−869.
(75) Kim, D.; Kim, E.; Park, S.; Kim, S.; Min, B. K.; Yoon, H. J.; Kwak, K.; Cho, M. Wettability of Graphene and Interfacial Water Structure. *Chem.* **2021**, *7*, 1602−1614.
(76) Frisenda, R.; Navarro-Moratalla, E.; Gant, P.; Pérez De Lara, D.; Jarillo-Herrero, P.; Gorbachev, R. V.; Castellanos-Gomez, A. Recent Progress in the Assembly of Nanodevices and Van Der Waals Heterostructures by Deterministic Placement of 2D Materials. *Chem. Soc. Rev.* **2018**, *47*, 53−68.
(77) He, F.; Zhou, Y.; Ye, Z.; Cho, S.-H.; Jeong, J.; Meng, X.; Wang, Y. Moiré Patterns in 2D Materials: A Review. *ACS Nano* **2021**, *15*, 5944−5958.
(78) Pirkle, A.; Chan, J.; Venugopal, A.; Hinojos, D.; Magnuson, C. W.; McDonnell, S.; Colombo, L.; Vogel, E. M.; Ruoff, R. S.; Wallace, R. M. The Effect of Chemical Residues on the Physical and Electrical Properties of Chemical Vapor Deposited Graphene Transferred to SiO_2. *Appl. Phys. Lett.* **2011**, *99*, 122108.
(79) Crameri, F.; Shephard, G. E.; Heron, P. J. The Misuse of Colour in Science Communication. *Nat. Commun.* **2020**, *11*, 5444.
(80) Momma, K.; Izumi, F. VESTA 3 for Three-Dimensional Visualization of Crystal, Volumetric and Morphology Data. *J. Appl. Crystallogr.* **2011**, *44*, 1272−1276.

NOTE ADDED AFTER ASAP PUBLICATION

This paper was published on December 7, 2022. There was an error in Figure 5, which has been corrected. The revised version was published on December 27, 2022.

https://doi.org/10.1021/acsnano.2c06963
ACS Nano 2022, 16, 20521−20532